

Chapter 2

Rechargeable Sensor Networks with Magnetic Resonant Coupling

Liguang Xie[†], Yi Shi[†], Y. Thomas Hou^{†*}, Wenjing Lou[†],
Hanif D. Sherali[†], and Huaibei Zhou[‡]

[†]*Virginia Polytechnic Institute and State University,
Blacksburg, Virginia, USA*

[‡]*Wuhan University, Wuhan, Hubei, China*

{*xie, yshi, thou, wjlou, hanifs*}@vt.edu, *bzhou@whu.edu.cn*

1. Introduction

Existing wireless sensor networks (WSNs) are constrained by limited battery energy at a sensor node. To save energy for sensor nodes and prolong network lifetime, there have been active research efforts at all layers, from topology control, physical, media access control (MAC), and all the way up to the application layer (see, e.g., [1; 4; 6; 16; 17]). Despite these intensive efforts, the energy and lifetime problems of a WSN remain a performance bottleneck and are a key factor that hinders its wide-scale deployment.

Recently, *magnetic resonant coupling (MRC)*, a novel wireless power transfer (WPT) technology that transfers electric power from one storage device to another *without any plugs or wires*, was developed by Kurs *et al.* [7]. It offers a new opportunity for addressing energy and lifetime problems for a WSN. Basically, Kurs *et al.*'s work showed that by exploiting magnetic resonance induction, WPT is both feasible and practical. In addition to WPT, they showed that the source device does not need to be in contact with the receiving device (e.g., a distance of 2 meters) for efficient power transfer. Moreover, MRC is insensitive to the neighboring environment and does not require a line of sight (LOS) between the source and receiving nodes. Recent advances in this technology further showed that it

*For correspondence, please contact Prof. Tom Hou (thou@vt.edu).

can be made portable, with applications to palm size devices such as cell phones [5].

Clearly, the impact of MRC is immense. To date, MRC has already been applied to charge batteries in medical sensors and implanted devices [25], where battery replacement is impractical. MRC has also been applied to recharge mobile devices (e.g. cell phones, tablets, laptops) and electric/hybrid vehicles.

Inspired by the new MRC technology, this chapter re-examines the energy and lifetime paradigms for a WSN.^a We review recent advances of MRC technology, and study several interesting cases to which this new technology can be applied to address the energy and lifetime problems in WSNs.

1.1. *Magnetic Resonant Coupling: A Primer*

The MRC technology is based on the well-known principle of resonant coupling, i.e., by having magnetic resonant coils operate at the same resonance frequency so that they are strongly coupled via nonradiative magnetic resonance induction. Intuitively, the effect of magnetic resonance is analogous to the classical mechanical resonance, under which a string, when tuned to a certain tone, can be excited to vibration by a faraway sound generator if there is a match between their resonance frequencies.

Under resonant coupling, energy can be transferred efficiently from a source coil to a receiver coil while losing little energy to extraneous off-resonant objects. A highlight of Kurs' experiment was to power a 60-W light bulb from a distance of 2 meters away, with about 40% power transfer efficiency (see Fig. 1 (a)). The diameter of both source and receiving coils was 0.5 m, which means that the charging distance can be 4 times the coil diameter.

There are some significant advantages of MRC technology over other WPT technologies [22]. Compared to inductive coupling, MRC can achieve higher efficiency in power transfer while significantly extending the charging distance (from a distance less than the coil diameter, usually several centimeters, to several times the coil diameter, e.g., 2 meters in Kurs' experiments). Compared to electromagnetic radiation, MRC has the advantages of offering a much higher power transfer efficiency even under omni-

^aAnother technology to address energy problem for a WSN is energy harvesting [13], e.g., solar, wind, vibrations, and ambient radio signals. Energy-harvesting technologies are orthogonal to MRC technology. Since energy harvesting has been discussed extensively in other chapters, we will not discuss it in this chapter.



Fig. 1. (a) MRC was first demonstrated by Kurs *et al.* [7]. (b) Intel proposed wireless power system by using flat coils (URL: <http://www.intel.com>). (c) Witricity demonstrated MRC for cell phones [5]. (d) Haier HDTV was powered by wireless electricity [11].

direction, not requiring LOS, and being insensitive to weather conditions.

Since the first demo by Kurs *et al.* in 2007, there have been some new advances in MRC to make it suitable for commercial applications. In 2008 (see Fig. 1 (b)), engineers at Intel demonstrated MRC by using flat coils, which are easier to fit into a mobile device than the helix coils used in [7]. Kurs *et al.* launched a start-up company called Witricity Corp. [18], and at the TED Global 2009 conference (see Fig. 1 (c)), they demonstrated MRC for portable devices such as cell phones [5]. Further, Kurs *et al.* developed an enhanced technology (by properly tuning coupled resonators) that allows energy to be transferred to multiple receiving coils at the same time [8]. This technology allows for broader home and office applications, e.g., charging multiple mobile devices (laptops, tablets, cell phones) simultaneously.

In 2010 (see Fig. 1(d)), home appliance maker Haier exhibited an all wireless HDTV without power cords and signal cables [11]. More recently, several leading automakers (e.g. Rolls-Royce, Audi, Nissan, Toyota, Mitsubishi) have been working to power electric or plug-in hybrid vehicles wirelessly. In 2011, Rolls-Royce unveiled an electric version of its Phantom car. The development of MRC technology allows these electric vehicles to be charged while they are parked along the street or in a garage without any power cord. This MRC technology, once fully mature, could help boost the electric car industry.

1.2. Chapter Organization

The remainder of this chapter is organized as follows. In Section 2, we show how MRC can be applied to remove the lifetime performance bottleneck of a WSN. We show that, through periodic recharging with a wireless charging vehicle (WCV), each sensor node can have an energy level above a minimum threshold so that the WSN can remain operational forever. In Section 3, we show how MRC with multi-charging technology can be used to address scalability problem for WPT in a WSN. In Sections 2 and 3, we assume that the location of the base station is fixed. On the other hand, it has been well recognized that a mobile base station can offer significant advantages over a fixed one. In Section 4, we explore how to co-locate the mobile base station on the WCV. Section 5 summarizes this chapter.

Table 1 lists notation used in this chapter.

Table 1. Notation.

Symbol	Definition
a_i (\hat{a}_i)	Arrival time of the WCV at node i in the first renewable cycle (or the initial transient cycle)
a_k^c	Arrival time of the WCV at cell k in the first cycle
B	Base station
C_{ij} (or C_{iB})	Energy consumption for transmitting one unit of data rate from node i to node j (or the base station B)
$C_{iB}(p(t))$	Energy consumption for transmitting one unit of data rate from node i to B when B is at location $p(t)$
D_{ij}	Distance from node i and node j
D_δ	WCV's charging range
D_i^c	Distance from node i to its cell center
$D_{\mathcal{P}}$	Distance of path \mathcal{P}
D_{TSP}	Minimum traveling distance in the shortest Hamiltonian cycle that connects the service station and sensor nodes
D_{TSP}^c	Minimum traveling distance in the shortest Hamiltonian cycle that connects the service station and the centers of cell $k \in \mathcal{Q}$
$D_{iB}(p)$	Distance between sensor node i and the WCV when the WCV is located at $p \in \mathcal{P}$
E_{max}	Full battery capacity at a sensor node
E_{min}	Minimum energy required to keep a sensor node operational
E_i	Starting energy of node i in a renewable cycle
$e_i(t)$	Energy level of sensor node i at time t
f_{ij} (or f_{iB})	Flow rate from sensor node i to sensor node j (or base station B)
$f_{ij}(t)$ (or $f_{iB}(t)$)	Flow rate from sensor node i to sensor node j (or base station B) at time t
\mathcal{N}	The set of sensor nodes in the network
\mathcal{N}_k	The set of sensor nodes in the k -th cell
\mathcal{P}	Traveling path of the WCV in a cycle
$p(t)$	Location of the base station B at time t

Table 1. (continued)

Symbol	Definition
\mathcal{Q}	The set of cells with at least one sensor node
R_i	Data rate generated at sensor node i
r_i	Energy consumption rate at sensor node i
$r_i(t)$	Energy consumption rate at sensor node i at time t
S	Service station
u_i	Charging rate at node i during the initial transient cycle
U	Energy transfer rate of the WCV in the renewable energy cycles
U_{\max}	Maximum output power from the WCV to charge a single sensor node
U_i	Power reception rate at sensor node i
$U_{iB}(p)$	Power reception rate at sensor node i when the WCV is located at $p \in \mathcal{P}$
V	Traveling speed of the WCV
(x_i, y_i)	Coordinates of node i
α	Path loss index
β_1	A constant in energy consumed for data transmission
β_2	A coefficient in energy consumed for data transmission
ρ	Power consumption coefficient for receiving data
δ	A threshold for a sensor's power reception rate
ϵ	Targeted performance gap ($0 < \epsilon \ll 1$)
η_k	Ratio of the charging time at cell k to the cycle time
η_{vac}	Ratio of the vacation time to the cycle time
τ	Cycle time
τ_i	Amount of time that the WCV spends to charge node i
τ_{vac}	Vacation time at the service station S
$\tau_{\mathcal{P}}$	WCV's traveling time on path \mathcal{P} in a cycle
τ_{TSP}	Minimum traveling time of the WCV in a cycle that connects the service station and sensor nodes
τ_{TSP}^c	Minimum traveling time of the WCV in a cycle that connects the service station and the centers of cell $k \in \mathcal{Q}$
ω_k	Amount of time that the WCV stays at the center of cell k
$\omega(p)$	Aggregate amount of time the WCV stops at point $p \in \mathcal{P}$
$\mu(d)$	Power transfer efficiency from the WCV to a sensor node that is at a distance d away

2. Single-Node Charging for a Sparse WSN

In this section, we investigate on how MRC technology can be applied and charge each sensor node so as to remove the lifetime bottleneck of a sparse WSN.

2.1. Problem Description

We consider a set of sensor nodes \mathcal{N} distributed over a two-dimensional area (see Fig. 2). Each sensor node has a battery capacity of E_{\max} and

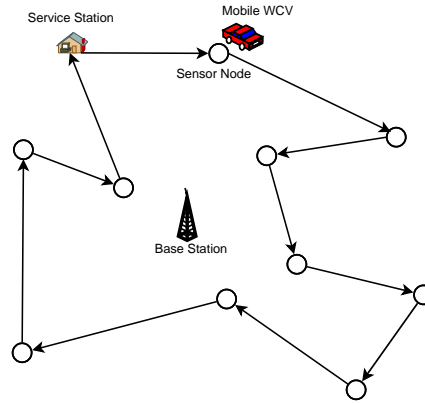


Fig. 2. A WCV periodically visits each sensor node and charges its battery via MRC.

is fully charged initially. Also, denote E_{\min} as the minimum energy at a sensor node battery (for it to be operational). For simplicity, we define network lifetime as the time until the energy level of any sensor node in the network falls below E_{\min} [1; 14; 17].

Each sensor node i generates sensing data with a rate of R_i (in b/s), $i \in \mathcal{N}$. Within the sensor network, there is a fixed base station (B), which is the sink node for data generated by all sensor nodes. Multi-hop data routing is employed for forwarding data by the sensor nodes. Denote f_{ij} as the flow rate from sensor node i to sensor node j and f_{iB} as the flow rate from sensor node i to the base station B , respectively. Then we have the following flow balance constraint at each node i :

$$\sum_{k \in \mathcal{N}}^{k \neq i} f_{ki} + R_i = \sum_{j \in \mathcal{N}}^{j \neq i} f_{ij} + f_{iB} \quad (i \in \mathcal{N}). \quad (1)$$

At a sensor node, we assume that communications (i.e., data transmission and reception) are the dominant source for the node's energy consumption. Denote r_i as the energy consumption rate at sensor node $i \in \mathcal{N}$. In this section, we use the following power consumption model [1; 6]:

$$r_i = \rho \sum_{k \in \mathcal{N}}^{k \neq i} f_{ki} + \sum_{j \in \mathcal{N}}^{j \neq i} C_{ij} f_{ij} + C_{iB} f_{iB} \quad (i \in \mathcal{N}), \quad (2)$$

where ρ is the energy consumption for receiving one unit of data rate, C_{ij} (or C_{iB}) is the energy consumption for transmitting one unit of data rate from node i to node j (or the base station B). Further, $C_{ij} = \beta_1 + \beta_2 D_{ij}^\alpha$, where D_{ij} is the distance between nodes i and j , β_1 is a distance-independent

constant term, β_2 is a coefficient of the distance-dependent term, and α is the path loss index. In the model, $\rho \sum_{k \in \mathcal{N}}^{k \neq i} f_{ki}$ is the energy consumption rate for reception, and $\sum_{j \in \mathcal{N}}^{j \neq i} C_{ij} f_{ij} + C_{iB} f_{iB}$ is the energy consumption rate for transmission.

To recharge the battery at each sensor node, a mobile wireless charging vehicle (WCV) is employed in the network. The WCV starts from a service station (S), and its traveling speed is V (in m/s). When it arrives at a sensor node, say i , it will spend τ_i amount of time to charge the node's battery wirelessly via MRC [7]. Denote U as the energy transfer rate of the WCV. After τ_i , the WCV leaves node i and travels to the next node on its path. We assume that the WCV has sufficient energy to charge all sensor nodes in the network. After the WCV visits all the sensor nodes in the network, it will return to its service station for maintenance (e.g., replacing or recharging its battery) and get ready for the next tour. We call this resting period *vacation time*, denoted as τ_{vac} . After this vacation, the WCV will go out for its next trip. Denote τ as the total time for the WCV to complete one cycle (including vacation).

A number of questions need to be answered for such a network. First, is it possible to have each sensor node never run out of its energy? If this is possible, then a WSN will have unlimited lifetime and will remain operational indefinitely. Second, is there any optimal plan (including traveling path, stopping schedule) such that some objective can be maximized or minimized? For example, we would like to minimize the percentage of time in a cycle that the WCV is out in the field, or equivalently, to maximize the percentage of time that the WCV is on vacation (i.e., $\frac{\tau_{\text{vac}}}{\tau}$).

2.2. Renewable Energy Cycles

As discussed, we assume that the WCV starts from the service station, visits each sensor node once in a cycle and ends at its service station (see Fig. 2). Further, we assume that the data flow routing in the network is invariant with time, although both routing and flow rates are part of an optimization problem.

Let $\mathcal{P} = (\pi_0, \pi_1, \dots, \pi_N, \pi_0)$ be the physical path traversed by the WCV over a trip, which starts from and ends at the service station (i.e., $\pi_0 = S$) and the i th node traversed by the WCV in a cycle is π_i , $1 \leq i \leq |\mathcal{N}|$. Denote $D_{\pi_0 \pi_1}$ as the distance between the service station and the first sensor node visited along \mathcal{P} and $D_{\pi_k \pi_{k+1}}$ as the distance between the k th and $(k+1)$ th sensor nodes, respectively. Denote a_i as the arrival time of the WCV at

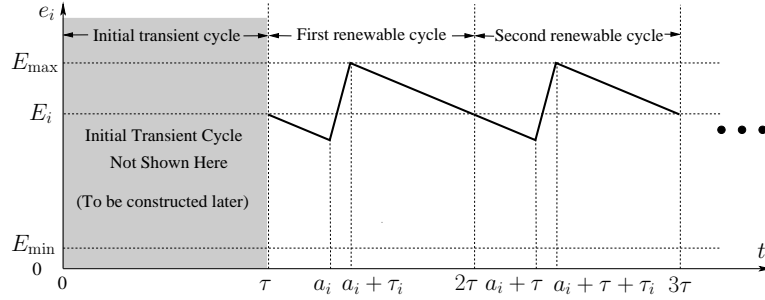


Fig. 3. The energy level of a sensor node i during the first two renewable cycles.

node i in the first renewable energy cycle (see Fig. 3). We have

$$a_{\pi_i} = \tau + \sum_{k=0}^{i-1} \frac{D_{\pi_k} \pi_{k+1}}{V} + \sum_{k=1}^{i-1} \tau_{\pi_k}. \quad (3)$$

Denote $D_{\mathcal{P}}$ as the physical distance of path \mathcal{P} and $\tau_{\mathcal{P}} = D_{\mathcal{P}}/V$ as the time spent for traveling over distance $D_{\mathcal{P}}$. Recall that τ_{vac} is the vacation time the WCV spends at its service station. Then the cycle time τ can be written as

$$\tau = \tau_{\mathcal{P}} + \tau_{\text{vac}} + \sum_{i \in \mathcal{N}} \tau_i, \quad (4)$$

where $\sum_{i \in \mathcal{N}} \tau_i$ is the total amount of time the WCV spends near all the sensor nodes in the network for WPT.

The energy level of a sensor node $i \in \mathcal{N}$ exhibits a renewable energy cycle if it meets the following two requirements: (i) it starts and ends with the same energy level over a period of τ ; and (ii) it never falls below E_{\min} .

During a renewable cycle, the amount of charged energy at a sensor node i during τ_i must be equal to the amount of energy consumed in the cycle (so as to ensure the first requirement for a renewable cycle). That is,

$$\tau \cdot r_i = \tau_i \cdot U \quad (i \in \mathcal{N}). \quad (5)$$

The sawtooth graph in Fig. 3 shows the energy level of a sensor node i during the first two renewable cycles. Note that there is an initialization cycle (in the grey area) before the first renewable cycle. That initialization cycle will be constructed later in Section 2.5 once we have a solution to the renewable cycles. For this energy curve in Fig. 3, denote E_i as the starting energy of node i in a renewable cycle and $e_i(t)$ as the energy level at time t , respectively. During a cycle $[\tau, 2\tau]$, we see that the energy level has only two slopes: (i) a slope of $-r_i$ when the WCV is not at this node, and (ii) a

slope of $(U - r_i)$ when the WCV is charging this node at a rate of U . Note that the battery energy is charged to E_{\max} during a WCV's visit.

Since the energy level at node i is at its lowest at time a_i , to ensure the second requirement for renewable energy cycle, we must have $e_i(a_i) = E_i - (a_i - \tau)r_i \geq E_{\min}$. Since for a renewable cycle,

$$\begin{aligned} E_i &= e_i(2\tau) = e_i(a_i + \tau_i) - (2\tau - a_i - \tau_i)r_i \\ &= E_{\max} - (2\tau - a_i - \tau_i)r_i, \end{aligned} \quad (6)$$

we have $e_i(a_i) = E_{\max} - (2\tau - a_i - \tau_i)r_i - (a_i - \tau)r_i = E_{\max} - (\tau - \tau_i)r_i$. Therefore,

$$E_{\max} - (\tau - \tau_i) \cdot r_i \geq E_{\min} \quad (i \in \mathcal{N}). \quad (7)$$

To construct a renewable energy cycle, we need to consider the traveling path \mathcal{P} , the arrival time a_i , the starting energy E_i , the flow rates f_{ij} and f_{iB} , time intervals τ , τ_i , $\tau_{\mathcal{P}}$, and τ_{vac} , and power consumption r_i . By (3) and (6), a_i and E_i are variables that can be derived from \mathcal{P} , τ , and τ_i . Thus, a_i and E_i can be excluded from a solution φ . So we have $\varphi = (\mathcal{P}, f_{ij}, f_{iB}, \tau, \tau_i, \tau_{\mathcal{P}}, \tau_{\text{vac}}, r_i)$.

In our recent work [19], we showed that Constraints (4), (5), and (7) are sufficient and necessary conditions for a renewable energy cycle. That is, a cycle is a renewable energy cycle if and only if Constraints (4), (5), and (7) are satisfied at each sensor node $i \in \mathcal{N}$. We also found an interesting property: in an optimal solution, there exists at least one energy "bottleneck" node in the network, where the energy level at this node drops exactly to E_{\min} upon the WCV's arrival [19].

2.3. Optimal Traveling Path

In an optimal solution with the maximum $\frac{\tau_{\text{vac}}}{\tau}$, we found that the WCV must travel along the shortest Hamiltonian cycle that connects all the sensor nodes and the service station [19]. The shortest Hamiltonian cycle can be obtained by solving the well known Traveling Salesman Problem (TSP) (see, e.g., [2; 12]). Denote D_{TSP} as the traveling distance in the shortest Hamiltonian cycle and let $\tau_{\text{TSP}} = D_{\text{TSP}}/V$. Then with the optimal traveling path, (4) becomes

$$\tau_{\text{TSP}} + \tau_{\text{vac}} + \sum_{i \in \mathcal{N}} \tau_i = \tau, \quad (8)$$

and the solution becomes $\varphi = (\mathcal{P}_{\text{TSP}}, f_{ij}, f_{iB}, \tau, \tau_i, \tau_{\text{TSP}}, \tau_{\text{vac}}, r_i)$. Since the optimal traveling path is determined, the solution can be simplified as $\varphi = (f_{ij}, f_{iB}, \tau, \tau_i, \tau_{\text{vac}}, r_i)$.

We note that the shortest Hamiltonian cycle may not be unique. Since any shortest Hamiltonian cycle has the same total path distance and traveling time τ_{TSP} , the selection of a particular shortest Hamiltonian cycle does not affect constraint (8), and yields the same optimal objective.

We also note that to travel the shortest Hamiltonian cycle, there are two (opposite) outgoing directions for the WCV to start from its home service station. Since the starting direction for the WCV does not affect constraint (8), either direction will yield an optimal solution with the same objective value, although some variables in each optimal solution will have different values.

2.4. Problem Formulation

Summarizing the objective and all the constraints, our Single-node Charging Problem (SCP) can be formulated as follows:

$$\begin{aligned}
 & \text{SCP} \\
 & \text{maximize} \quad \frac{\tau_{\text{vac}}}{\tau} \\
 & \text{subject to} \quad \text{Time constraint: (8);} \\
 & \quad \quad \quad \text{Flow routing constraints: (1);} \\
 & \quad \quad \quad \text{Energy consumption model: (2);} \\
 & \quad \quad \quad \text{Renewable energy cycle constraints: (5), (7);} \\
 & \quad \quad \quad f_{ij}, f_{iB}, \tau_i, \tau, \tau_{\text{vac}}, r_i \geq 0 \quad (i, j \in \mathcal{N}, i \neq j).
 \end{aligned}$$

In this problem, flow rates f_{ij} and f_{iB} , time intervals τ , τ_i , and τ_{vac} , and power consumption r_i are optimization variables, and R_i , ρ , C_{ij} , C_{iB} , U , E_{max} , E_{min} , and τ_{TSP} are constants. This problem has both nonlinear objective ($\frac{\tau_{\text{vac}}}{\tau}$) and nonlinear terms ($\tau \cdot r_i$ and $\tau_i \cdot r_i$) in Constraints (5) and (7). Problem SCP is a nonlinear program (NLP), and is NP-hard in general. In our recent work [19], we showed that a near-optimal solution to SCP can be achieved via a piecewise linear approximation technique. We refer readers to the reference[19] for more details.

2.5. An Initial Transient Cycle

In Section 2.2, we skipped the discussion on how to construct an initial transient cycle before the first renewable cycle. Unlike a renewable energy cycle at node i , which starts and ends with the same energy level E_i , the initial transient cycle starts with E_{max} and ends with E_i .

Now with the optimal traveling path \mathcal{P} (the shortest Hamiltonian cycle)

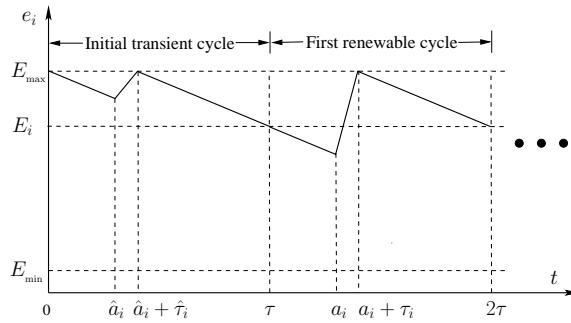


Fig. 4. Illustration of energy behavior for the initial transient cycle and how it connects to the first renewable cycle.

and the feasible near-optimal solution $(f_{ij}, f_{iB}, \tau, \tau_i, \tau_{vac}, r_i)$, we are ready to construct an initial transient cycle. Specifically, for a solution $\varphi = (\mathcal{P}, f_{ij}, f_{iB}, \tau, \tau_i, \tau_{vac}, r_i, U)$ corresponding to a renewable energy cycle for $t \geq \tau$, we construct $\hat{\varphi} = (\hat{\mathcal{P}}, \hat{f}_{ij}, \hat{f}_{iB}, \hat{\tau}, \hat{\tau}_i, \hat{\tau}_{vac}, \hat{r}_i, u_i)$ for the initial transient cycle for $t \in [0, \tau]$ by letting $\hat{\mathcal{P}} = \mathcal{P}$, $\hat{f}_{ij} = f_{ij}$, $\hat{f}_{iB} = f_{iB}$, $\hat{\tau} = \tau$, $\hat{\tau}_i = \tau_i$, $\hat{\tau}_{vac} = \tau_{vac}$, $\hat{r}_i = r_i$ and $u_i = \frac{r_i \hat{a}_i}{\tau_i} + r_i$, where u_i is the charging rate at node i during the initial transient cycle and \hat{a}_i is the arrival time of the WCV at node i in the initial transient cycle (see Fig. 4). In our recent work [19], we showed that this newly constructed $\hat{\varphi}$ is a feasible transient cycle.

2.6. An Example

We present an example to demonstrate how our solution can produce a renewable WSN and some interesting properties with such a network. We consider a randomly generated WSN consisting of 50 nodes. The sensor nodes are deployed over a square area of $1 \text{ km} \times 1 \text{ km}$. The data rate (i.e., R_i , $i \in \mathcal{N}$) from each node is randomly generated within $[1, 10]$ kb/s. The power consumption coefficients are $\beta_1 = 50 \text{ nJ/b}$, $\beta_2 = 0.0013 \text{ pJ}/(\text{b} \cdot \text{m}^4)$, $\alpha = 4$, and $\rho = 50 \text{ nJ/b}$ [6]. The base station is assumed to be located at $(500, 500)$ (in m) and the home service station for the WCV is assumed to be at the origin. The traveling speed of the WCV is $V = 5 \text{ m/s}$.

For the battery at a sensor node, we choose a regular NiMH battery and its nominal cell voltage and electricity volume is $1.2 \text{ V}/2.5 \text{ Ah}$. We have $E_{\max} = 1.2 \text{ V} \times 2.5 \text{ A} \times 3600 \text{ sec} = 10.8 \text{ KJ}$ [9]. We let $E_{\min} = 0.05 \cdot E_{\max} = 540 \text{ J}$. We assume the wireless energy transfer rate $U = 5 \text{ W}$ [7]. We set

Table 2. Location and data rate R_i for each node in a 50-node network.

Node Index	Location (m)	R_i (kb/s)	Node Index	Location (m)	R_i (kb/s)
1	(815, 276)	1	26	(758, 350)	9
2	(906, 680)	8	27	(743, 197)	1
3	(127, 655)	4	28	(392, 251)	4
4	(913, 163)	6	29	(655, 616)	4
5	(632, 119)	3	30	(171, 473)	9
6	(98, 498)	7	31	(706, 352)	5
7	(278, 960)	3	32	(32, 831)	10
8	(547, 340)	7	33	(277, 585)	1
9	(958, 585)	6	34	(46, 550)	3
10	(965, 224)	8	35	(97, 917)	2
11	(158, 751)	5	36	(823, 286)	2
12	(971, 255)	1	37	(695, 757)	8
13	(957, 506)	4	38	(317, 754)	6
14	(485, 699)	10	39	(950, 380)	6
15	(800, 891)	2	40	(34, 568)	2
16	(142, 959)	9	41	(439, 76)	8
17	(422, 547)	5	42	(382, 54)	7
18	(916, 139)	10	43	(766, 531)	4
19	(792, 149)	1	44	(795, 779)	6
20	(959, 258)	5	45	(187, 934)	6
21	(656, 841)	3	46	(490, 130)	1
22	(36, 254)	10	47	(446, 569)	3
23	(849, 814)	1	48	(646, 469)	2
24	(934, 244)	8	49	(709, 12)	2
25	(679, 929)	8	50	(755, 337)	3

the target performance gap (of our near-optimal solution) as 0.01 for the numerical results, i.e., our solution has an error no more than 0.01.

Table 2 gives the location of each node and its data rate for a 50-node network. The shortest Hamiltonian cycle is found by using the Concorde solver [2] and is shown in Fig. 5. For this optimal cycle, $D_{\text{TSP}} = 5821$ m and $\tau_{\text{TSP}} = 1164.2$ s. In our solution, the cycle time $\tau = 30.73$ hours, the vacation time $\tau_{\text{vac}} = 26.82$ hours, and the objective $\eta_{\text{vac}} = 87.27\%$.

As discussed in Section 2.3, the WCV can follow either direction of the shortest Hamiltonian cycle while achieving the same objective value $\eta_{\text{vac}} = 87.27\%$. Comparing the two solutions, the values for f_{ij} , f_{iB} , τ , τ_i , τ_{TSP} , τ_{vac} are identical although the values of a_i and E_i are different. This observation can be verified by the simulation results in Table 3 (counter clockwise direction) and Table 4 (clockwise direction). As an example, Figs. 6(a) and 6(b) show the energy cycle behavior of a sensor node (the

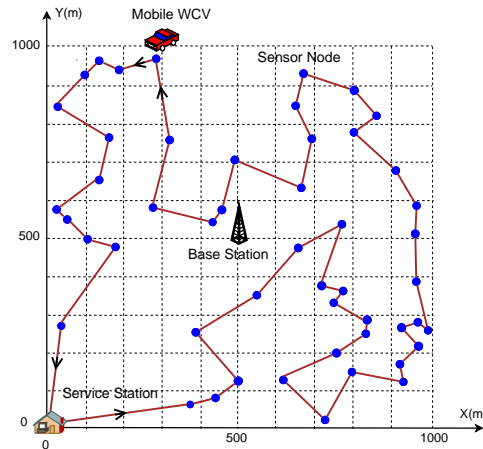


Fig. 5. An optimal traveling path for the WCV for the 50-node sensor network, assuming traveling direction is counter clockwise.

32th node) under the two opposite traveling directions, respectively.

As discussed in Section 2.2, there exists an energy bottleneck node in the network (with its energy dropping to E_{\min} during a renewable energy cycle). The bottleneck node in this network is the 48th node, whose energy behavior is shown in Fig. 7. In addition, Fig. 8 shows that data routing in our solution differs from the minimum energy routing for the 50-node network.

3. Multi-Node Charging for a Dense WSN

In Section 2, we first applied the MRC technology to a WSN and showed that through periodic power transfer, a WSN could remain operational indefinitely. An open problem in Section 2 is scalability of wireless charging. That is, as the node density increases in a WSN, how does the WCV charge each node in a timely manner before it runs out of energy?

Kurs *et al.* also recognized this problem and recently developed an enhanced MRC technology (by properly tuning coupled resonators) that allows energy to be transferred to *multiple* receiving nodes simultaneously [8]. Motivated by this new advance in WPT, in this section, we focus on addressing the scalability problem in charging a WSN with the multi-node charging technology.

Table 3. The case of counter clockwise traveling direction: Node visited along the path, arrival time at each node, starting energy of each node in a renewable cycle, and charging time at each node for the 50-node network.

Node Order	a_i (s)	E_i (J)	τ_i (s)	Node Order	a_i (s)	E_i (J)	τ_i (s)
42	110702	10747	11	2	117778	10611	41
41	110725	10613	37	44	117848	10605	42
46	110777	9282	305	23	117903	10793	2
28	111113	7697	627	15	117923	10747	11
8	111776	7590	653	25	117960	10685	25
48	112461	714	2092	21	118002	10593	44
43	114579	10594	43	37	118065	8827	425
31	114660	6233	957	29	118519	8493	499
26	115627	10752	10	14	119056	10299	109
50	115639	9851	199	47	119192	10581	47
36	115855	10137	139	17	119246	9246	338
1	115997	9594	254	33	119614	4961	1287
27	116273	10551	53	38	120936	10059	164
5	116353	10646	33	7	121142	10754	10
49	116412	10610	40	45	121171	10658	31
19	116484	10660	29	16	121213	10738	14
18	116538	10622	38	35	121239	10259	120
4	116581	10329	100	32	121380	8628	483
10	116696	10596	43	11	121894	10010	176
24	116747	9648	245	3	122090	6697	924
20	116997	10773	6	40	123039	10790	2
12	117006	10794	1	34	123046	10747	12
39	117032	8565	477	6	123073	10519	63
13	117534	10020	167	30	123151	8319	563
9	117717	10613	40	22	123766	5722	1166

3.1. Mathematical Modeling

Following the setting in Section 2, we consider a WCV periodically traveling inside the WSN, making stops and charging sensor nodes near these stops. Upon completing each trip, the WCV returns to its home service station, takes a “vacation”, and starts out for its next trip. In contrast to Section 2, the WCV is now capable of charging multiple nodes at the same time, as long as these nodes are within its charging range, denoted as D_δ . The charging range D_δ is determined by having the power reception rate at a sensor node be at least over a threshold (denoted as δ). The power reception rate at a sensor node i , denoted as U_i , is a distance-dependent parameter, and decreases with the distance between node i and the WCV. When a

Table 4. The case of clockwise traveling direction: Node visited along the path, arrival time at each node, starting energy of each node in a renewable cycle, and charging time at each node for the 50-node network.

Node Order	a_i (s)	E_i (J)	τ_i (s)	Node Order	a_i (s)	E_i (J)	τ_i (s)
22	110676	5032	1166	9	117852	10613	40
30	111894	8032	563	13	117907	10023	167
6	112472	10489	63	39	118099	8588	477
34	112550	10741	12	12	118601	10795	1
40	112567	10789	2	20	118605	10773	6
3	112594	6301	924	24	118617	9668	245
11	113538	9944	176	10	118868	10600	43
32	113744	8461	483	4	118928	10339	100
35	114250	10222	120	18	119032	10626	38
16	114382	10734	14	19	119095	10664	29
45	114406	10648	31	49	119156	10615	40
7	114456	10751	10	5	119223	10650	33
38	114508	10012	164	27	119283	10558	53
33	114706	4676	1287	1	119357	9632	254
17	116024	9197	338	36	119613	10160	139
47	116368	10575	47	50	119770	9888	199
14	116443	10286	109	26	119972	10754	10
29	116590	8449	499	31	119992	6464	957
37	117118	8809	425	43	120986	10606	43
21	117561	10593	44	48	121056	1526	2092
25	117624	10685	25	8	123180	7927	653
15	117674	10747	11	28	123868	8059	627
23	117703	10793	2	46	124526	9472	305
44	117718	10605	42	41	124846	10637	37
2	117789	10611	41	42	124896	10754	11

sensor node is more than a distance of D_δ away from the WCV, we assume that its power reception rate is too low to make MRC work properly at the sensor node's battery. D_δ can be determined by [8], which will be given in Section 3.3.

We introduce a logical cellular structure and assume that the WCV can only stop at the center of a cell. Specifically, we partition the two-dimensional plane with hexagonal cells with a side length of D_δ (see Fig. 9). Therefore, when the WCV makes a stop at the center of a cell, all sensor nodes in the cell can be charged simultaneously. We ignore the edge effect where a sensor node residing outside the cell but inside a circle with a radius of D_δ can still be charged from this cell. Note that such omission of

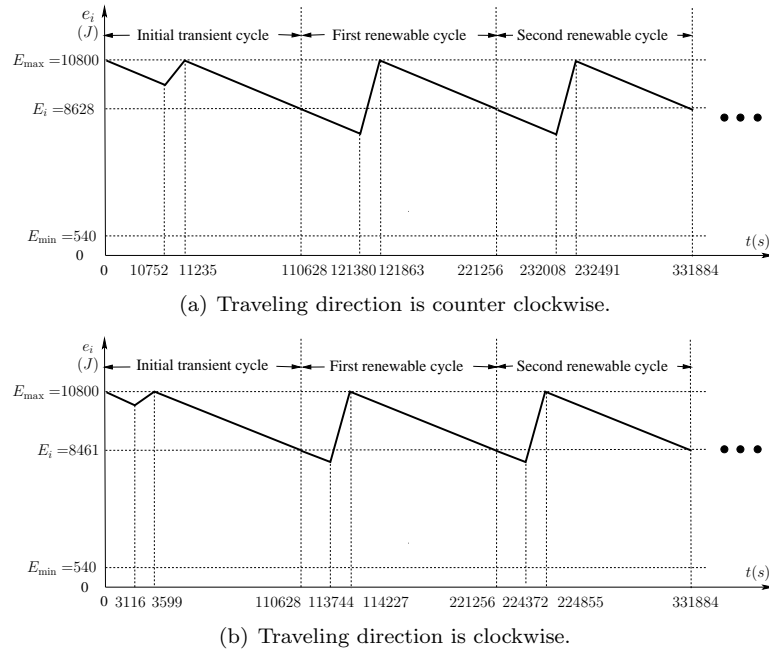


Fig. 6. The energy behavior of a sensor node (the 32th) in the 50-node network during the initial transient cycle and the first two renewable cycles.

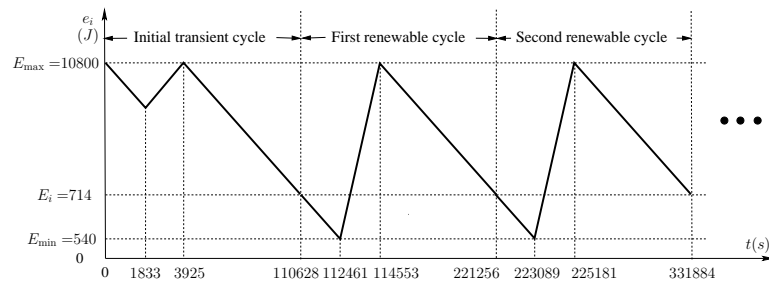
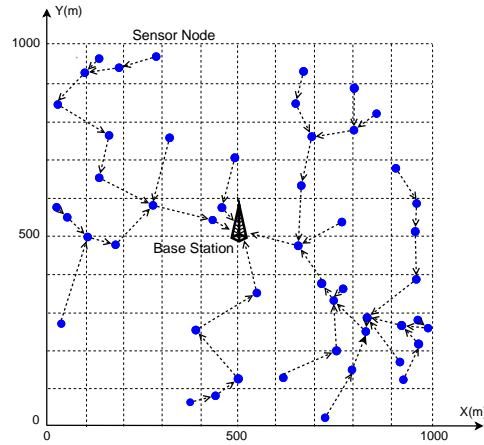


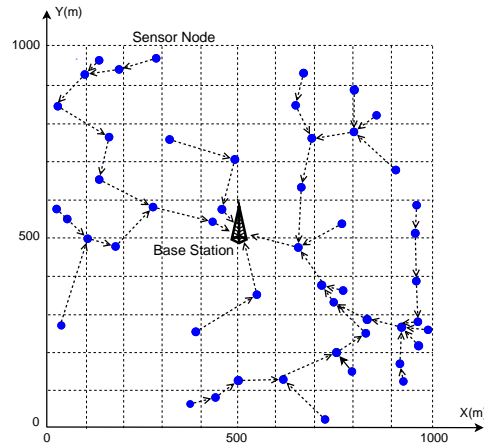
Fig. 7. The energy behavior of the bottleneck node (48th node) in the 50-node network. Traveling direction is counter clockwise.

over-charging will not affect the feasibility of our solution.

Under the cellular structure, denote D_i^c the distance from node i to its cell center. Then nodes i 's power reception rate is $U_i = \mu(D_i^c) \cdot U_{\max}$, where U_{\max} is the maximum output power from the WCV for a single sensor node



(a) Data routing in our solution.



(b) Minimal energy routing.

Fig. 8. A comparison of data routing by our solution and that by minimum energy routing for the 50-node network.

and $\mu(D_i^c)$ is the WPT efficiency. Note that $\mu(D_i^c)$ is a decreasing function of D_i^c and $0 \leq \mu(D_i^c) \leq 1$.

Denote \mathcal{Q} as the set of hexagonal cells containing at least one sensor node (see Fig. 10). Re-index these cells in \mathcal{Q} as $k = 1, 2, \dots, |\mathcal{Q}|$ and denote \mathcal{N}_k as the set of sensor nodes in the k th cell. Then $\mathcal{N} = \bigcup_{k \in \mathcal{Q}} \mathcal{N}_k$.

Denote ω_k as the time that the WCV stays at the center of cell $k \in$

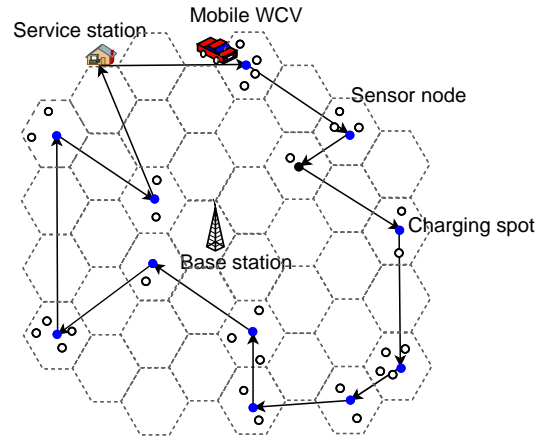


Fig. 9. An example sensor network with a mobile WCV. Solid dots represent cell centers and empty circles represent sensor nodes.

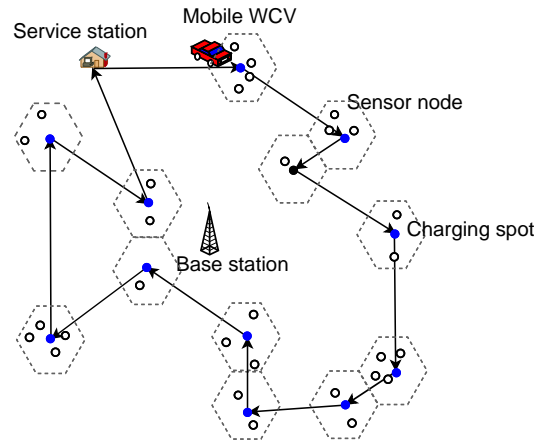


Fig. 10. An example sensor network with a WCV. Only those cells with sensor nodes are shown in this figure.

\mathcal{Q} . Throughout ω_k , the WCV re-charges all sensor nodes within this cell simultaneously via multi-node charging technology [8]. After ω_k , the WCV leaves the current cell and travels to the next cell on its path. In our formulation, we assume that the WCV visits a cell only once during a cycle. Let $\mathcal{P} = (\phi_0, \phi_1, \dots, \phi_{|\mathcal{Q}|}, \phi_0)$ be the physical path traversed by the WCV during a cycle, which starts from and ends at the service station

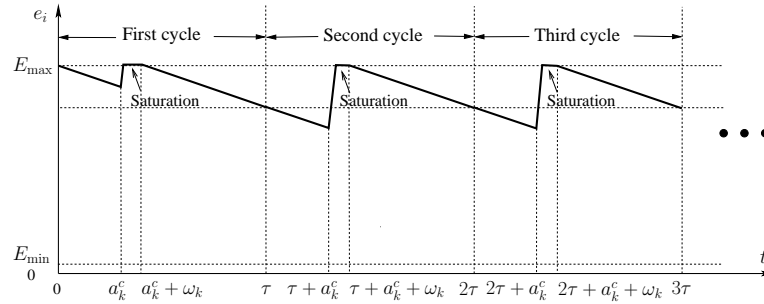


Fig. 11. The energy level of node $i \in \mathcal{N}_k$ during the first three cycles. a_k^c is the arrival time of the WCV at cell k in the first cycle.

(i.e., $\phi_0 = S$) and the k th cell traversed by the WCV along path \mathcal{P} is ϕ_k , $1 \leq k \leq |\mathcal{Q}|$. Recall that $D_{\mathcal{P}}$ is the physical distance of path \mathcal{P} and $\tau_{\mathcal{P}} = D_{\mathcal{P}}/V$ is the time spent for traveling over distance $D_{\mathcal{P}}$.

After the WCV visits the $|\mathcal{Q}|$ cells in the network, it will return to its service station. Then this cycle time τ can be written as

$$\tau = \tau_{\mathcal{P}} + \tau_{\text{vac}} + \sum_{k \in \mathcal{Q}} \omega_k, \quad (9)$$

where τ is the cycle time, τ_{vac} is the vacation time, and $\sum_{k \in \mathcal{Q}} \omega_k$ is the total amount of time the WCV spends at the $|\mathcal{Q}|$ cells for battery charging.

In Section 2, we considered a WCV visiting each node and charging it individually. In that context, we introduced a concept, namely *renewable energy cycle*, during which the energy level at each node exhibits a periodic behavior with a cycle time τ . A central idea in achieving a renewable energy cycle in Section 2 is that the amount of energy being charged to a node is equal to the amount of energy that the node expends in a cycle. However, such an idea cannot be extended to our multi-node charging context here. This is because, for each node in the same cell, its remaining energy level (when the WCV arrives at the cell) differs, so do energy charging rate and consumption rate at each node. As a result, nodes in the same cell will not complete their battery charging at the same time and those nodes that finish early will run into a “saturation” state (i.e., battery level remains at E_{max}) until the WCV departs this cell (see Fig. 11). Due to this “saturation” phenomenon, the idea of achieving a renewable energy cycle cannot be applied here.

We now develop constraints to capture the saturation phenomena while ensuring that the energy level of each node never falls below E_{min} . Denote a_k^c as the arrival time of the WCV at cell k in the first cycle, and recall that

$e_i(t)$ is node i 's energy level at time t . The energy curve of node $i \in \mathcal{N}_k$ in a cell k for the first three cycles is shown in Fig. 11. For any cycle, we see that there can be only three possible slopes: (i) a slope of $-r_i$ when the WCV is not in node i 's cell, (ii) a slope of $(U_i - r_i)$ when the WCV is at node i 's cell and is charging node i at rate U_i , and (iii) a slope of 0 (i.e., saturation period) when node i is already fully charged while the WCV is still in the same cell.

Since the energy level of node i is no more than E_{\max} at the beginning of a cycle, to ensure that $e_i(t) \geq E_{\min}$ for all $t \geq 0$, we must have

$$E_{\max} - (\tau - \omega_k) \cdot r_i \geq E_{\min} \quad (i \in \mathcal{N}_k, k \in \mathcal{Q}), \quad (10)$$

where $(\tau - \omega_k) \cdot r_i$ is the amount of energy consumed by node i when the WCV is out of its cell k during a cycle.

Note that (10) is a necessary condition for $e_i(t) \geq E_{\min}$. The following is another necessary condition for $e_i(t) \geq E_{\min}$.

$$\tau \cdot r_i - U_i \cdot \omega_k \leq 0 \quad (i \in \mathcal{N}_k, k \in \mathcal{Q}), \quad (11)$$

which says that $U_i \cdot \omega_k$, the amount of energy being charged to node $i \in \mathcal{N}_k$ during the time period of ω_k , must be greater than or equal to $\tau \cdot r_i$, the amount of energy consumed during the cycle.

Recently, we showed that (10) and (11) are also sufficient conditions [20]. That is, $e_i(t) \geq E_{\min}$ for all $t \geq 0$, $i \in \mathcal{N}$, if and only if both constraints (10) and (11) are satisfied. In addition, we showed that each sensor node $i \in \mathcal{N}_k$ is fully charged to E_{\max} when the WCV departs cell k , $k \in \mathcal{Q}$ [20].

3.2. Problem Formulation and Properties

We consider minimizing energy consumption of the entire system, which encompasses all energy consumption on the WCV. Since the energy consumed to carry the WCV to move along \mathcal{P} is the dominant source of energy consumption (when compared its wireless charging to sensor nodes), we aim to minimize the fraction of time that the WCV is at work (outside its service station), i.e., $\frac{\tau_{\mathcal{P}} + \sum_{k \in \mathcal{Q}} \omega_k}{\tau}$. It is interesting that, by (9), minimizing $\frac{\tau_{\mathcal{P}} + \sum_{k \in \mathcal{Q}} \omega_k}{\tau}$ is equivalent to maximizing $\frac{\tau_{\text{vac}}}{\tau}$, which is the percentage of time that the WCV is on vacation at its service station.

We now summarize our optimization problem as follows.

$$\begin{aligned}
& \text{maximize} && \frac{\tau_{\text{vac}}}{\tau} \\
& \text{subject to} && \text{Time constraint: (9);} \\
& && \text{Flow routing constraints: (1);} \\
& && \text{Energy consumption model: (2);} \\
& && \text{Cell-based energy constraints: (10), (11);} \\
& && \tau, \tau_{\mathcal{P}}, \tau_{\text{vac}}, \omega_k, f_{ij}, f_{iB} \geq 0 \quad (i, j \in \mathcal{N}, i \neq j); \\
& && 0 \leq r_i \leq U_i \quad (i \in \mathcal{N}).
\end{aligned}$$

This problem is a NLP, with nonlinear objective ($\frac{\tau_{\text{vac}}}{\tau}$) and nonlinear terms ($\tau \cdot r_i$ and $\omega_k \cdot r_i$) in constraints (10) and (11). An NLP is NP-hard in general. Nevertheless, we can still find several useful properties associated with an optimal solution.

In our prior work [20], we showed that in an optimal solution with the maximal $\frac{\tau_{\text{vac}}}{\tau}$, the WCV must move along the shortest Hamiltonian cycle that connects the service station and the centers of cells $k \in \mathcal{Q}$. Denote D_{TSP}^c as the total path distance for the shortest Hamiltonian cycle and $\tau_{\text{TSP}}^c = D_{\text{TSP}}^c/V$. Then (9) becomes

$$\tau - \sum_{k \in \mathcal{Q}} \omega_k - \tau_{\text{vac}} = \tau_{\text{TSP}}^c. \quad (12)$$

For (12), we divide both sides by τ and have $1 - \sum_{k \in \mathcal{Q}} \frac{\omega_k}{\tau} - \frac{\tau_{\text{vac}}}{\tau} = \tau_{\text{TSP}}^c \cdot \frac{1}{\tau}$. We define $\eta_{\text{vac}} = \frac{\tau_{\text{vac}}}{\tau}$, where η_{vac} denotes the ratio of the vacation time to the cycle time. Similarly, we define $\eta_k = \frac{\omega_k}{\tau}$, for $k \in \mathcal{Q}$, and $h = \frac{1}{\tau}$, where η_k denotes the ratio of the charging time at cell k to the cycle time. Then (12) is written as $1 - \sum_{k \in \mathcal{Q}} \eta_k - \eta_{\text{vac}} = \tau_{\text{TSP}}^c \cdot h$, or equivalently, $h = \frac{1 - \sum_{k \in \mathcal{Q}} \eta_k - \eta_{\text{vac}}}{\tau_{\text{TSP}}^c}$.

Similarly, by dividing both sides by τ , replacing $\frac{\omega_k}{\tau}$ with η_k , and replacing $\frac{1}{\tau}$ with $\frac{1 - \sum_{k \in \mathcal{Q}} \eta_k - \eta_{\text{vac}}}{\tau_{\text{TSP}}^c}$, (10) and (11) can be reformulated as:

$$(1 - \eta_k) \cdot r_i \leq (E_{\text{max}} - E_{\text{min}}) \cdot \frac{1 - \sum_{j \in \mathcal{Q}} \eta_j - \eta_{\text{vac}}}{\tau_{\text{TSP}}^c} \quad (i \in \mathcal{N}_k, k \in \mathcal{Q}), \quad (13)$$

$$r_i - U_i \cdot \eta_k \leq 0 \quad (i \in \mathcal{N}_k, k \in \mathcal{Q}). \quad (14)$$

Now Multi-node Charging Problem (MCP) is reformulated as follows:

MCP

$$\begin{aligned}
& \text{maximize} && \eta_{\text{vac}} \\
& \text{subject to} && \text{Flow routing constraints: (1);} \\
& && \text{Energy consumption model: (2);} \\
& && \text{Cell-based energy constraints: (13), (14);} \\
& && f_{ij}, f_{iB} \geq 0, 0 \leq r_i \leq U_i, 0 \leq \eta_k, \eta_{\text{vac}} \leq 1 \quad (i, j \in \mathcal{N}, i \neq j).
\end{aligned}$$

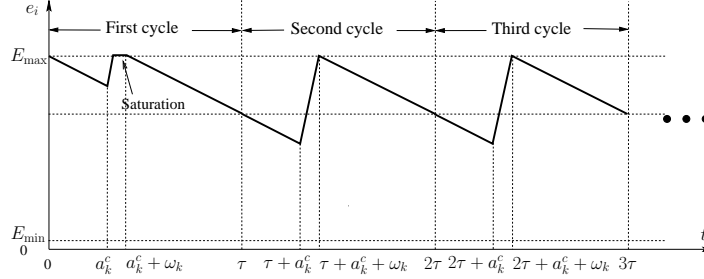


Fig. 12. The energy level of an equilibrium node $i \in \mathcal{N}_k$ in the first three cycles.

In this problem, f_{ij} , f_{iB} , r_i , η_{vac} , and η_k are optimization variables; R_i , ρ , C_{ij} , C_{iB} , U_i , E_{max} , E_{min} and τ_{TSP}^c are constants. Once we obtain a solution to problem MCP, we can recover τ , ω_k , and τ_{vac} as follows: $\tau = \frac{\tau_{TSP}^c}{1 - \sum_{k \in \mathcal{Q}} \eta_k - \eta_{vac}}$, $\omega_k = \tau \cdot \eta_k$, and $\tau_{vac} = \tau \cdot \eta_{vac}$.

In our prior work [20], we found that in an optimal solution to MCP, there exists at least one *bottleneck node*, which is the node whose energy level drops exactly to E_{min} upon WCV's arrival. As discussed, when the WCV departs cell k , $k \in \mathcal{Q}$, each sensor node in this cell is fully charged to E_{max} . Further, some nodes may experience saturation state during each cycle. In our prior work [20], we found that in an optimal solution, at least one sensor node in each cell $k \in \mathcal{Q}$ has saturation-free cycles except its initial first cycle (see Fig. 12). We call such a node as *equilibrium node*.

Problem MCP is nonconvex [3], and cannot be solved by existing off-the-shelf solvers. In our prior work [20], we showed that a near-optimal solution to MCP can be developed via a technique called Reformulation-Linearization Technique (RLT) [15].

3.3. An Example

We present a 100-node network to demonstrate our proposed solution. We also demonstrate how our solution can address the scalability issue when the density of sensor nodes increases.

The network setting follows that in Section 2.6. That is, sensor nodes are deployed over a 1 km \times 1 km square area. The base station is at (500, 500) (in m) and the WCV's home service station is assumed to be at the origin. The traveling speed of the WCV is $V = 5$ m/s. The data rate R_i , $i \in \mathcal{N}$, from each node is randomly generated within [1, 10] kb/s. The

Table 5. Location and data rate R_i for each node in a 100-node network.

Node index	Location (m)	R_i (kb/s)	Node index	Location (m)	R_i (kb/s)
1	(140.8,905.4)	3	51	(613.9,474.1)	9
2	(977.8,913.0)	5	52	(837.1,6.1)	2
3	(679.9,92.7)	4	53	(635.8,216.4)	4
4	(325.8,378.1)	5	54	(165.7,109.6)	7
5	(196.2,526.8)	8	55	(634.9,218.4)	1
6	(546.5,967.0)	2	56	(747.2,33.2)	7
7	(323.4,329.4)	7	57	(821.4,608.6)	5
8	(747.7,33.4)	3	58	(250.1,839.1)	10
9	(838.3,678.0)	1	59	(990.6,617.0)	6
10	(692.5,461.4)	9	60	(977.9,909.0)	4
11	(918.4,517.9)	1	61	(585.6,623.4)	5
12	(613.6,476.1)	1	62	(678.6,91.7)	1
13	(586.2,621.8)	4	63	(613.5,475.9)	1
14	(440.2,17.7)	4	64	(438.8,17.3)	2
15	(813.3,749.9)	7	65	(836.5,680.4)	10
16	(886.2,612.7)	7	66	(321.9,331.2)	3
17	(804.9,329.4)	5	67	(752.3,714.6)	9
18	(633.7,218.4)	4	68	(679.6,93.7)	8
19	(753.3,713.0)	9	69	(838.0,677.4)	6
20	(163.7,108.6)	2	70	(897.2,709.2)	2
21	(672.0,318.1)	10	71	(750.8,712.4)	3
22	(250.2,840.1)	1	72	(635.5,217.4)	7
23	(732.3,965.0)	4	73	(585.4,622.0)	6
24	(197.4,672.2)	6	74	(732.0,966.2)	3
25	(92.7,967.7)	1	75	(91.5,971.3)	2
26	(990.1,617.4)	4	76	(918.6,514.1)	2
27	(804.3,352.0)	7	77	(166.0,109.0)	8
28	(821.5,609.8)	7	78	(90.6,967.7)	10
29	(898.3,708.4)	6	79	(813.4,749.7)	1
30	(688.4,59.1)	3	80	(686.9,59.7)	10
31	(837.3,4.5)	2	81	(587.1,622.4)	2
32	(451.2,135.5)	1	82	(838.2,680.4)	4
33	(979.3,911.8)	8	83	(249.7,842.5)	3
34	(678.9,93.3)	8	84	(139.9,902.0)	7
35	(751.6,714.2)	6	85	(691.4,459.4)	3
36	(633.8,217.0)	9	86	(747.3,36.0)	5
37	(452.9,133.7)	3	87	(803.9,327.0)	7
38	(633.6,217.8)	1	88	(164.6,108.4)	3
39	(884.4,613.9)	1	89	(197.8,670.4)	5
40	(197.1,523.2)	6	90	(820.8,610.2)	3
41	(813.8,747.7)	5	91	(140.8,904.6)	9
42	(804.1,326.6)	4	92	(546.3,965.4)	4
43	(732.9,966.2)	3	93	(886.8,613.1)	8
44	(690.1,460.2)	7	94	(671.5,318.9)	8
45	(669.9,319.1)	7	95	(248.7,842.9)	4
46	(195.9,670.2)	10	96	(670.6,318.1)	7
47	(440.7,17.1)	2	97	(613.3,477.1)	9
48	(670.2,319.3)	10	98	(614.2,475.7)	5
49	(585.1,624.2)	1	99	(452.2,133.1)	7
50	(896.5,708.4)	8	100	(197.4,670.6)	4

power consumption coefficients β_1 , β_2 , ρ , and α are the same as that in Section 2.6.

For the battery at a sensor node, we have $E_{\max} = 10.8$ kJ, and $E_{\min} = 0.05 \cdot E_{\max} = 540$ J. For $\mu(D_i^c)$, we refer to the experimental data on WPT

Table 6. Cells index, location of cell center, sensor nodes in each cell, cell traveling order along the path, and charging time at each cell for the 100-node network.

Cell index	Location of cell center (m)	Sensor nodes in the cell	Travel order	τ_k (s)
1	(140.4, 904.1)	1, 84, 91	26	157
2	(452.3, 134.8)	32, 37, 99	2	314
3	(837.0, 6.2)	31, 52	6	157
4	(687.1, 60.0)	30, 80	4	157
5	(897.8, 710.1)	29, 50, 70	21	157
6	(820.8, 609.5)	28, 57, 90	17	628
7	(804.6, 352.3)	27	10	157
8	(990.9, 618.9)	26, 59	20	157
9	(91.8, 969.6)	25, 75, 78	25	157
10	(197.1, 670.3)	24, 46, 89, 100	28	2510
11	(731.7, 964.9)	23, 43, 74	23	314
12	(249.8, 841.0)	22, 58, 83, 95	27	471
13	(670.9, 317.2)	21, 45, 48, 94, 96	8	314
14	(164.7, 109.1)	20, 54, 77, 88	32	471
15	(751.9, 714.7)	19, 35, 67, 71	14	314
16	(634.5, 216.7)	18, 36, 38, 53, 55, 72	7	157
17	(804.6, 328.9)	17, 42, 87	9	157
18	(885.6, 614.2)	16, 39, 93	18	157
19	(812.7, 749.8)	15, 41, 79	15	157
20	(440.1, 15.6)	14, 47, 64	1	157
21	(585.9, 623.5)	13, 49, 61, 73, 81	13	157
22	(614.3, 476.2)	12, 51, 63, 97, 98	12	314
23	(918.0, 516.0)	11, 76	19	157
24	(691.2, 459.9)	10, 44, 85	11	157
25	(837.0, 679.7)	9, 65, 69, 82	16	157
26	(747.9, 34.3)	8, 56, 86	5	157
27	(322.6, 331.3)	7, 66	31	2353
28	(545.4, 964.9)	6, 92	24	157
29	(197.1, 525.3)	5, 40	29	784
30	(326.7, 380.4)	4	30	157
31	(679.0, 92.8)	3, 34, 62, 68	3	157
32	(978.8, 911.1)	2, 33, 60	22	314

efficiency in [8]. Through curve fitting, we obtain $\mu(D_i^c) = -0.0958D_i^c \cdot D_i^c - 0.0377D_i^c + 1.0$. Assuming $U_{\text{Full}} = 5$ W and $\delta = 1$ W, we have $D_\delta = 2.7$ m for a cell's side length. We set the target performance gap (of our near-optimal solution) as 0.1 for the numerical results.

We first present complete results for a 100-node network. Table 5 gives the location of each node and its data rate for the 100-node network. These

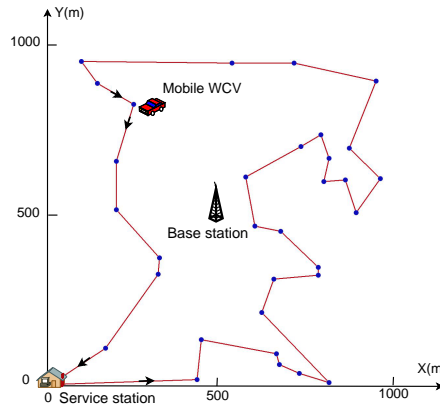


Fig. 13. An optimal traveling path (assuming counter clockwise direction) for the 100-node sensor network. The 100 nodes are distributed in 32 cells, with the center of each cell being represented as a point in the figure.

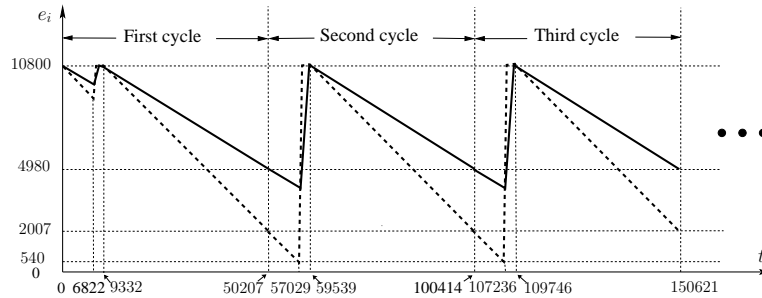


Fig. 14. Energy cycle behavior of an equilibrium node (node 24, in solid curve) and a non-equilibrium node (node 89, in dashed curve) in the 100-node network. Node 89 is also a bottleneck node.

100 nodes are distributed in $|\mathcal{Q}| = 32$ selected cells and Table 6 gives the location of each cell as well as the number of sensor nodes it contains. The shortest Hamiltonian cycle that threads all cells $k \in \mathcal{Q}$ and the service station is found by the Concorde TSP solver [2], which is shown in Fig. 13. For this optimal cycle, $D_{TSP}^c = 5110$ m and $\tau_{TSP}^c = 1022$ s ≈ 0.28 h. We have cycle time $\tau = 13.95$ h, vacation time $\tau_{vac} = 10.26$ h, total charging time $13.95 - 10.26 - 0.28 = 3.41$ h, and the objective $\eta_{vac} = 73.55\%$.

In Section 3.1, we showed that each sensor node in the network is fully charged to E_{max} when the WCV departs its cell, which is confirmed by our

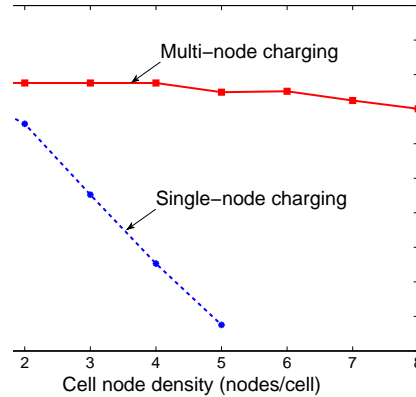


Fig. 15. Achievable objective value as a function of node density under multi-node and single-node charging technologies.

numerical results. In Section 3.2, we showed that in an optimal solution, there exists at least one equilibrium node in each cell $k \in \mathcal{Q}$. In our numerical results, all 32 cells contain equilibrium nodes.

To examine energy behavior at sensor nodes, consider sensor nodes in cell 10. There are 4 sensor nodes in this cell, nodes 24 and 46 are equilibrium nodes while nodes 89 and 100 are not. Fig. 14 shows the energy behavior of node 24 (solid curve) and node 89 (dashed curve). Note that node 24 does not have any saturation period except in the initial first cycle while node 89 has saturation period in every cycle.

In Section 3.2, we showed that there exists an energy bottleneck node in the network with its energy dropping to E_{\min} during a cycle. This is also confirmed in our numerical results. The bottleneck node is the 89th node, whose energy behavior is shown in Fig. 14.

Now we demonstrate how multi-node charging can address the scalability problem for WPT. We consider $|\mathcal{Q}| = 25$ cells and increase node density in these cells from 1 to 8 per cell. For each density, we compare multi-node charging with single-node charging. Fig. 15 shows the numerical results. We have two observations: (i) The achievable objective value under multi-node charging remains steady when node density increases from 1 to 8, with only slight decrease. On the other hand, the achievable objective value under single-node charging drops very quickly when node density increases and a feasible solution does not exist when node density is beyond 5. (ii) Over the entire density range (from 1 to 8), the objective value under

Table 7. Details of comparison between multi-node charging and single-node charging.

Density (Nodes/Cell)	Multi-node Charging			Single-node Charging		
	τ (h)	$\sum_{k \in Q} \tau_k$ (h)	η_{vac}	τ (h)	$\sum_{k \in Q} \tau_k$ (h)	η_{vac}
1	8.28	1.59	77.59%	8.12	1.84	75.58%
2	8.27	1.59	77.58%	4.72	1.46	65.75%
3	8.22	1.58	77.57%	7.32	3.86	45.24%
4	8.24	1.58	77.57%	5.64	4.06	25.29%
5	7.21	1.76	74.91%	6.20	5.58	7.54%
6	8.28	1.79	75.19%	–	–	–
7	7.33	1.75	72.50%	–	–	–
8	6.83	1.77	70.11%	–	–	–

multi-node charging is always higher than that under single-node charging and the gap between them widens as density increases.

Table 7 gives more details for the study shown in Fig. 15. Note that under multi-node charging, the achievable objective value at density 6 is slightly larger than that at density 5. This local fluctuation is due to more possibilities for routing when density increases. However, this is only a local fluctuation. The prevailing trend is that η_{vac} decreases as density increases.

4. Bundling Mobile Base Station and Magnetic Resonant Coupling

In Sections 2 and 3, we have shown that MRC is a promising technology to fundamentally address energy and lifetime problems in a WSN. Note that in Sections 2 and 3, although the WCV is mobile, the base station in the WSN (sink node for all sensing data) is fixed. On the other hand, it has been well recognized that a *mobile* base station (MBS) can achieve significant energy saving and network lifetime extension [10; 16; 23]. Given that a MBS needs to be carried on a vehicle, we explore the possibility of having the base station co-locate on the same vehicle used for carrying the wireless charger.

When there is no ambiguity, we still call the combined systems as WCV. The WCV starts from its home service station, travels along a pre-planned path and returns to its home service station at the end of a trip. While traveling on its path, the WCV can make a number of stops and charge sensor nodes near those stops. At any time, all data collected by the sensor nodes are relayed (via multi-hop) to the MBS (on WCV). A basic require-

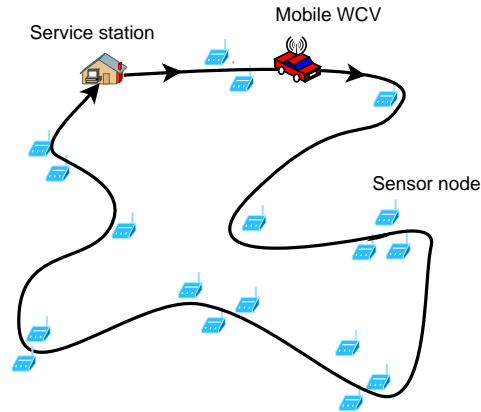


Fig. 16. A WCV that combines MBS and MRC traveling in a WSN.

ment is that by employing MRC, none of the sensor nodes shall run out of energy while all sensing data are relayed to the base station in real time. A second goal is to minimize energy consumption of the entire system.

4.1. Mathematical Modeling and Problem Formulation

We develop a mathematical model for co-locating the MBS on the WCV. In addition, we offer energy criteria to ensure that the energy level at each sensor node never falls below E_{\min} . Further, we provide a general optimization problem formulation.

A WCV is employed to charge sensor nodes in the network. This WCV starts from a service station, travels along a pre-planned path in the area and returns to the service station at the end of its trip. Along its path, the WCV makes a number of stops and charges sensor nodes near those stops (see Fig. 16).

Recall that \mathcal{P} is the traveling path and τ is the total amount of time for the WCV to complete the trip. Then τ includes three components:

- The total traveling time along path \mathcal{P} is $D_{\mathcal{P}}/V$.
- The vacation time τ_{vac} at the service station (located at point p_{vac}).
- The total stopping time along path \mathcal{P} . Denote $\omega(p)$ as the aggregate amount of time the WCV stops at point $p \in \mathcal{P}$. Since the WCV may stop at p more than once during τ , we have:

$$\omega(p) = \int_{\{t \in [0, \tau] : (x, y)(t) = p\}} 1 \, dt \quad (p \in \mathcal{P}), \quad (15)$$

where $(x, y)(t)$ is the location of the WCV at time t . Then the total stopping time is $\sum_{p \in \mathcal{P}, p \neq p_{\text{vac}}}^{\omega(p) > 0} \omega(p)$.

Then we have:

$$\tau = \frac{D_{\mathcal{P}}}{V} + \tau_{\text{vac}} + \sum_{p \in \mathcal{P}, p \neq p_{\text{vac}}}^{\omega(p) > 0} \omega(p). \quad (16)$$

Since the base station is co-located on the WCV, the base station is mobile. Denote $f_{ij}(t)$ and $f_{iB}(t)$ as the flow rates from node i to node j and the base station at time t , respectively. Then we have the following flow balance at each sensor node i :

$$\sum_{k \in \mathcal{N}}^{k \neq i} f_{ki}(t) + R_i = \sum_{j \in \mathcal{N}}^{j \neq i} f_{ij}(t) + f_{iB}(t) \quad (i \in \mathcal{N}). \quad (17)$$

Denote $C_{iB}(p(t))$ as the energy consumption rate for transmitting one unit of data flow from node i to base station B when B is at location $p(t)$. Then we have

$$C_{iB}(p(t)) = \beta_1 + \beta_2 \left[\sqrt{(x(t) - x_i)^2 + (y(t) - y_i)^2} \right]^\alpha \quad (i \in \mathcal{N}), \quad (18)$$

where $(x(t), y(t))$ and (x_i, y_i) are the coordinates of $p(t)$ and node i , respectively. Note that unlike C_{ij} 's, which are all constants, $C_{iB}(p(t))$ varies with the base station's location over time.

The total energy consumption rate for both transmission and reception at node i , denoted as $r_i(t)$, is

$$r_i(t) = \rho \sum_{k \in \mathcal{N}}^{k \neq i} f_{ki}(t) + \sum_{j \in \mathcal{N}}^{j \neq i} C_{ij} \cdot f_{ij}(t) + C_{iB}(p(t)) \cdot f_{iB}(t) \quad (i \in \mathcal{N}). \quad (19)$$

We assume that the WCV can only perform its charging function when it makes a full stop along path \mathcal{P} (except p_{vac}). Denote $U_{iB}(p)$ as the power reception rate at node i when the WCV is located at $p \in \mathcal{P}$. Then the WPT efficiency is $\mu(D_{iB}(p))$, which is a decreasing function of distance $D_{iB}(p)$, the distance between node i and the WCV when the WCV is located at $p \in \mathcal{P}$. Following the wireless charging model in [21], we have:

$$U_{iB}(p) = \begin{cases} \mu(D_{iB}(p)) \cdot U_{\text{max}} & \text{if } D_{iB}(p) \leq D_\delta \\ 0 & \text{if } D_{iB}(p) > D_\delta. \end{cases} \quad (20)$$

We are interested in developing a particular travel cycle so that $e_i(t)$, $i \in \mathcal{N}$, never falls below E_{min} . In the following, we will offer two constraints

for the *first* cycle. Once these two constraints hold for the first cycle, we can show that $e_i(t) \geq E_{\min}$ for $t \geq \tau$, i.e., all future cycles.

The first constraint ensures that $e_i(t)$, which starts from E_{\max} at $t = 0$, will not fall below E_{\min} at $t = \tau$,

$$E_{\max} - \left\{ \int_{\{t \in [0, \tau]: \omega(p(t))=0\}} r_i(t) dt + \int_{\{t \in [0, \tau]: \omega(p(t))>0, D_{iB}(p(t))>D_\delta\}} r_i(t) dt \right\} \geq E_{\min} \quad (i \in \mathcal{N}), \quad (21)$$

where $\int_{\{t \in [0, \tau]: \omega(p(t))=0\}} r_i(t) dt$ is the amount of energy consumed at node i when the WCV is moving along path \mathcal{P} while $\int_{\{t \in [0, \tau]: \omega(p(t))>0, D_{iB}(p(t))>D_\delta\}} r_i(t) dt$ is the amount of energy consumed at node i when the WCV is making stops but node i is outside the WCV's charging range.

The second constraint ensures that $e_i(t)$, which starts from E_{\max} at $t = 0$, will be charged back to E_{\max} before the end of the first cycle τ . We have

$$\int_0^\tau r_i(t) dt \leq \sum_{p \in \mathcal{P}}^{\omega(p)>0, D_{iB}(p) \leq D_\delta} U_{iB}(p) \cdot \omega(p) \quad (i \in \mathcal{N}), \quad (22)$$

where the left-hand-side is the amount of energy consumed at node i during τ and the right-hand-side is the maximum possible amount of energy received by node i in a cycle. Note that the actual amount of energy received by node i in the first cycle may be less than the right-hand-side due to potential battery overflow.

Note that (21) and (22) characterize the energy consumption and reception in the first cycle. Recently, we showed that if both (21) and (22) hold for the first cycle, then we have $e(t) \geq E_{\min}$ for all the cycles [21].

Similar to Sections 2 and 3, we want to minimize energy consumption of the entire system, which can be modeled as maximizing $\frac{\tau_{\text{vac}}}{\tau}$. Therefore, we have the following formulation for the WCV and mobile base station Co-location Problem based on time (CoP-t).

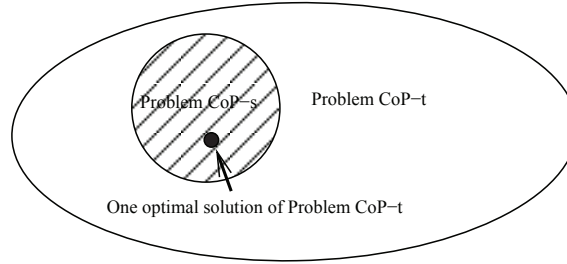


Fig. 17. Solution space for problems CoP-t and CoP-s.

CoP-t:

$$\begin{aligned}
 & \text{maximize} && \frac{\tau_{\text{vac}}}{\tau} \\
 & \text{s.t.} && \text{Time constraints: (15), (16);} \\
 & && \text{Flow routing constraints: (17);} \\
 & && \text{Energy consumption model: (18), (19);} \\
 & && \text{Energy criteria constraints: (21), (22);} \\
 & && \tau, \tau_{\text{vac}}, \omega(p) \geq 0, (x, y)(t) \in \mathcal{P} \quad (p \in \mathcal{P}, 0 \leq t \leq \tau); \\
 & && f_{ij}(t), f_{iB}(t), C_{iB}(t), r_i(t) \geq 0, (i, j \in \mathcal{N}, i \neq j, 0 \leq t \leq \tau).
 \end{aligned}$$

In this formulation, \mathcal{P} , $D_{\mathcal{P}}$, V , R_i , β_1 , β_2 , α , x_i , y_i , ρ , C_{ij} , E_{\max} , and E_{\min} are given *a priori*, and $U_{iB}(p)$ can be computed by (20). The time intervals τ , τ_{vac} , and $\omega(p)$, the WCV's location $(x, y)(t)$, the flow rates $f_{ij}(t)$ and $f_{iB}(t)$, the unit cost rate $C_{iB}(t)$, and the power consumption rate $r_i(t)$ are optimization variables. Among these variables, there are three sets of variables that constitute the solution space: (i) the WCV's location (i.e., $(x, y)(t)$); (ii) the WCV's sojourn time at each location $p \in \mathcal{P}$ and $p \neq p_{\text{vac}}$ (i.e., $\omega(p)$) or vacation time at the service station (i.e., τ_{vac}); (iii) the corresponding flow routing (i.e., $f_{ij}(t)$ and $f_{iB}(t)$). Problem CoP-t is a continuous-time nonlinear program [24], and is NP-hard in general.

4.2. Downsizing Solution Space: A Location-based Formulation

CoP-t is a general formulation of our problem. It is difficult as its variables are time-dependent (e.g., $(x, y)(t)$, $f_{ij}(t)$). In this general formulation, CoP-t allows data flow routing and energy consumption of sensor nodes to vary over time, even when the WCV visits the same location.

We consider a special case of problem CoP-t, where data flow routing and energy consumption of sensor nodes only depend on WCV's location.

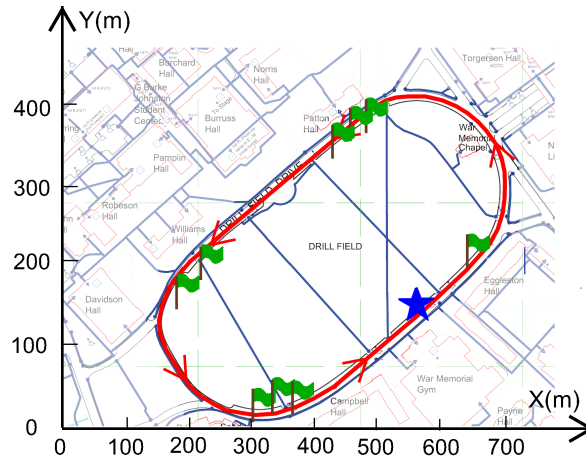


Fig. 18. Drillfield driveway on Virginia Tech campus. A star represents the WCV's home service station. A flag represents a stopping point in the example (Section 4.3).

That is, as long as the WCV visits a location $p \in \mathcal{P}$, the data flow routing and energy consumption of sensor nodes are the same regardless when the WCV visits this location. This location (space)-dependent problem is a special case of Problem CoP-t. We denote this problem as Co-location Problem based on space (CoP-s). The solution spaces for CoP-s and CoP-t are shown in Fig. 17, in which the solution space for CoP-s is completely contained in that for CoP-t.

In our recent work [21], we showed that the optimal objective value for CoP-s is the same as that for CoP-t, despite that its solution space is smaller. This result allows us to study CoP-s, which has a simpler formulation that only involves location-dependent variables.

Although CoP-s is simpler than CoP-t, path \mathcal{P} still has infinite number of points. In our recent work [21], we showed that by discretizing path \mathcal{P} into a finite number of segments and representing each segment as a *logical* point, we could develop a provably $(1 - \epsilon)$ near-optimal solution.

4.3. An Example

We use a 25-node network to demonstrate how our algorithm solves the WCV and mobile base station co-location problem. We use Virginia Tech's Drillfield (see Fig. 18) for sensor network deployment. Sensor nodes are

Table 8. Location and data rate R_i for each node in a 25-node network.

Node Index	Location (m)	R_i (Kb/s)	Node Index	Location (m)	R_i (Kb/s)
1	(626.0, 236.1)	1	14	(247.6, 181.6)	7
2	(623.3, 235.6)	7	15	(245.9, 180.4)	4
3	(624.0, 237.2)	1	16	(247.7, 181.0)	10
4	(625.6, 237.1)	1	17	(220.5, 118.0)	5
5	(460.8, 357.8)	1	18	(220.5, 121.1)	2
6	(462.6, 361.9)	4	19	(219.5, 119.8)	7
7	(459.8, 359.0)	2	20	(220.7, 118.3)	6
8	(461.1, 359.0)	3	21	(328.8, 12.2)	2
9	(435.7, 337.8)	2	22	(335.2, 13.2)	9
10	(433.3, 337.7)	4	23	(334.2, 13.0)	4
11	(435.2, 338.5)	5	24	(333.2, 13.9)	8
12	(434.8, 337.4)	5	25	(331.5, 13.7)	8
13	(245.1, 180.3)	1			

deployed within a distance of the charging range along the side of the Drillfield driveway, which is roughly an ellipse. The home service station (marked as a star in Fig. 18) is located at (540,160) (in m) along the driveway. For the Drillfield path \mathcal{P} , $D_{\mathcal{P}} = 1228$ m. The travel speed of the WCV is $V = 5$ m/s. The data rate R_i , $i \in \mathcal{N}$ for each node is randomly generated within [1, 10] Kb/s. The values of parameter E_{\max} , E_{\min} , β_1 , β_2 , ρ , α , U_{\max} , and δ , and the charging efficiency function $\mu(D_{iB})$ are the same as those in Section 3.3. We set $\epsilon = 0.05$.

We present results for a 25-node sensor network. The location of each node and its data rate are given in Table 8. In the solution, we have $\tau = 17.29$ h, $\tau_{\text{vac}} = 16.29$ h, and the objective value is 94.21%. Since the total traveling time along path \mathcal{P} is $1228/5 = 245.6$ s ≈ 0.07 h, we have that the total stopping time for charging is $17.29 - 16.29 - 0.07 = 0.93$ h.

Upon termination, there are a total of 316 segments (corresponding to 316 logical points). However, the WCV only makes 9 stops among these segments, and merely traverses the other segments without stop. For illustration purpose, we use a physical point (x, y) within the corresponding segment to represent the segment where the WCV makes a stop. These stopping points are marked with flags in Fig. 18, and the location and the amount of time at each stop are given in Table 9. Note that the number of stops for the WCV is much fewer than the number of sensor nodes due to multi-node charging. For example, the WCV charges nodes 1, 2, 3, and 4 at the same time when it stops at the 1st point (625.7, 235.3). Also, it

Table 9. Index of stopping point along the path, location and time spent at each stopping point for the 25-node network.

Visit Order	Location (m)	$\omega(p)$ (s)	Visit Order	Location (m)	$\omega(p)$ (s)
1	(625.7, 235.3)	23	6	(221.0, 119.4)	219
2	(461.1, 357.4)	358	7	(329.3, 11.9)	2
3	(464.5, 360.2)	9	8	(332.4, 12.1)	9
4	(435.4, 336.2)	98	9	(333.9, 12.4)	2318
5	(247.3, 179.3)	42			

is possible that a node may be charged more than once in a cycle. For example, node 25 is charged when the WCV stops at both the 8th point (332.4, 12.1) and the 9th point (333.9, 12.4).

5. Summary

In this chapter, we exploited the emerging MRC technology, and showed that it is a promising technology to address energy and lifetime problems in a WSN. We offered a review of MRC technology and its recent advances. We then studied three interesting cases with this charging technology. First, we investigated the question of whether MRC can be applied to remove the lifetime performance bottleneck of a sparse WSN. We showed that once properly designed, a WSN has the potential to remain operational forever. Based on this result, we exploited recent advances in multi-node MRC technology that allows multiple sensor nodes to be charged at the same time. We showed that multi-node charging could address the charging scalability problem in a dense WSN. Finally, we considered to bundle the base station and MRC together, and again studied how to charge sensor nodes for a WCV with a MBS on top.

References

1. J. Chang and L. Tassiulas, "Maximum lifetime routing in wireless sensor networks," *IEEE/ACM Trans. on Networking*, vol. 12, no. 4, pp. 609–619 (Aug. 2004).
2. Concorde TSP Solver, URL: <http://www.tsp.gatech.edu/concorde/>.
3. C.A. Floudas, *Deterministic Global Optimization: Theory, Methods, and Applications*, Chapter 2, Kluwer Academic (Dec. 1999).
4. A. Giridhar and P.R. Kumar, "Maximizing the functional lifetime of sensor

- networks,” in *Proc. ACM/IEEE International Symposium on Information Processing in Sensor Networks*, pp. 5–12, Los Angeles, CA (Apr. 2005).
5. E. Giler, “Eric Giler demos wireless electricity,” URL: http://www.ted.com/talks/eric_giler_demos_wireless_electricity.html.
 6. Y.T. Hou, Y. Shi, and H.D. Sherali, “Rate allocation and network lifetime problems for wireless sensor networks,” *IEEE/ACM Trans. on Networking*, vol. 16, no. 2, pp. 321–334 (Apr. 2008).
 7. A. Kurs, A. Karalis, R. Moffatt, J.D. Joannopoulos, P. Fisher, and M. Soljacic, “Wireless power transfer via strongly coupled magnetic resonances,” *Science*, vol. 317, no. 5834, pp. 83–86 (2007).
 8. A. Kurs, R. Moffatt, and M. Soljacic, “Simultaneous mid-range power transfer to multiple devices,” *Appl. Phys. Lett.*, vol. 96, no. 4, article 4102 (Jan. 2010).
 9. D. Linden and T.B. Reddy (eds.), *Handbook of Batteries*, Third Edition, Chapter 1, McGraw-Hill (2002).
 10. J. Luo and J.-P. Huabux, “Joint sink mobility and routing to maximize the lifetime of wireless sensor networks: The case of constrained mobility,” *IEEE/ACM Trans. on Networking*, vol. 18, no. 3, pp. 871–884 (June 2010).
 11. J. Messina, “Haier exhibits a wireless HDTV video system at the 2010 CES,” URL: <http://phys.org/news182608923.html>.
 12. M. Padberg and G. Rinaldi, “A branch-and-cut algorithm for the resolution of large-scale symmetric traveling salesman problems,” *SIAM Review*, vol. 33, no. 1, pp. 60–100 (1991).
 13. S. Priya and D.J. Inman (eds.), *Energy Harvesting Technologies*, New York, NY: Springer (2009).
 14. A. Sankar and Z. Liu, “Maximum lifetime routing in wireless ad-hoc networks,” in *Proc. IEEE INFOCOM*, pp. 1089–1097, Hong Kong, China, March 7–11 (Mar. 2004).
 15. H.D. Sherali, W.P. Adams and P.J. Driscoll, “Exploiting special structures in constructing a hierarchy of relaxations for 0-1 mixed integer problems,” *Operations Research*, vol. 46, no. 3, pp. 396–405 (1998).
 16. Y. Shi and Y.T. Hou, “Theoretical results on base station movement problem for sensor network,” in *Proc. IEEE INFOCOM*, pp. 376–384, Phoenix, AZ (Apr. 2008).
 17. W. Wang, V. Srinivasan, and K.C. Chua, “Extending the lifetime of wireless sensor networks through mobile relays,” *IEEE/ACM Trans. on Networking*, vol. 16, no. 5, pp. 1108–1120 (Oct. 2008).
 18. WiTricity Corp., URL: <http://www.witricity.com>.
 19. L. Xie, Y. Shi, Y.T. Hou, and H.D. Sherali, “Making sensor networks immortal: An energy-renewal approach with wireless power transfer,” *IEEE/ACM Trans. on Networking*, vol. 20, no. 6, pp. 1748–1761 (Dec. 2012).
 20. L. Xie, Y. Shi, Y.T. Hou, W. Lou, H.D. Sherali, and S. F. Midkiff, “On renewable sensor networks with wireless energy transfer: The multi-node case,” in *Proc. IEEE SECON*, Seoul, Korea, pp. 10–18 (June 2012).
 21. L. Xie, Y. Shi, Y.T. Hou, W. Lou, H.D. Sherali, and S. F. Midkiff, “Bundling mobile base station and wireless energy transfer: Modeling and optimiza-

36 *L. Xie, Y. Shi, Y.T. Hou, W. Lou, H.D. Sherali, and H. Zhou*

- tion,” in *Proc. IEEE INFOCOM*, Turin, Italy, April 14–19 (Apr. 2013).
22. L. Xie, Y. Shi, Y.T. Hou, and W. Lou, “Wireless power transfer and applications to sensor networks,” *IEEE Wireless Communications Magazine*, vol. 20, no. 4, pp. 140–145 (2013).
 23. G. Xing, T. Wang, W. Jia, and M. Li, “Rendezvous design algorithms for wireless sensor networks with a mobile base station,” in *Proc. ACM MobiHoc*, Hong Kong, China, May 27–30, pp. 231–240 (2008).
 24. G.J. Zalmi, “Optimality conditions and Lagrangian duality in continuous-time nonlinear programming,” *Journal of Mathematical Analysis and Applications*, vol. 109, no. 2, pp. 426–452 (Aug. 1985).
 25. F. Zhang, X. Liu, S.A. Hackworth, R.J. Scabassi, and M. Sun, “In vitro and in vivo studies on wireless powering of medical sensors and implantable devices,” in *Proc. IEEE/NIH Life Science Systems and Applications Workshop (LiSSA)*, pp. 84–87, Bethesda, MD (Apr. 2009).